Nuclear Physics A199 (1973) 193—217;

SHELL-MODEL ANALYSIS OF PAIRING EXCITATIONS IN THE REGION $52 \leqq A \leqq 60$

D. R. BES †, E. E. MAQUEDA † and R. P. J. PERAZZO †
Comisión Nacional de Energía Atómica, Departamento Física Nuclear, Av. Libertador 8250, Buenos Aires, Argentina

Received 14 August 1972

Abstract: A shell-model diagonalization of a $T = 1$ residual pairing interaction is performed in the vicinity of ^{56}Ni for $J^\pi = 0^+$ states. Energies and differential cross sections for two-body transfer processes are compared with experimental values and with the harmonic predictions. Special attention is paid to those reactions which are sensitive to the existence of a phase transition between normal and superconducting systems. Furthermore, it is shown that the assumption of a harmonic non-adiabatic addition phonon explains systematically a number of weak transitions. A list of spectroscopic amplitudes for relevant (and so far unreported) cross sections is included.

1. Introduction

The energies and two-particle transfer intensities to $J^\pi = 0^+$ states in the region $40 \leqq A \leqq 70$ may be understood [1-3]) using a $T = 1$ pairing residual interaction.

The main effects of this interaction can be described in terms of collective degrees of freedom [1, 4, 5]). These are easily treated in two limiting cases: if the strength G of the pairing interaction is sufficiently small, the $J^\pi = 0^+$ states are described in terms of addition and removal (harmonic) phonons carrying an isospin $t = 1$. The limit of large G gives rise to the pairing rotational scheme, in which a single intrinsic structure is assumed to rotate in both charge and gauge space.

Deviations from both theoretical predictions are experimentally observed [3, 6, 7]), and it is apparent that a transitional pattern is present.

Additional calculations [8]) attempt a consistent description of a large set of experimental evidence in this region by introducing phenomenological anharmonicities into a vibrational scheme.

A complementary method of dealing with a residual interaction like the pairing force is to perform an exact diagonalization in a suitable shell-model space. In a previous paper [9]) such a diagonalization has been performed in a two-level model with the aim of describing the gradual change from the vibrational to the rotational limit. The purpose of this paper is to bring that model calculation to a more realistic framework (by using actual single-particle levels), and thereafter to attempt a fit of the energy of $J^\pi = 0^+$ states and two-particle transfer cross sections in the vicinity of

† Fellow of the Consejo Nacional de Investigaciones Cientificas y Tecnicas.

$A = 56$. From this point of view, the present paper may be considered an extension of the calculation performed by Bayman and Hintz for the $|T_z| = 1$ pairing interaction [ref. [10])].

We also perform a comparison between the shell-model results and a calculation in terms of harmonic phonons. We conclude that a large fraction of the available experimental data in the vicinity of $A = 56$ can be adequately systematized within the harmonic description by including a non-adiabatic addition phonon plus the usual adiabatic addition and removal modes. We find, in fact, that the harmonic description is more suitable for the non-adiabatic phonon than for the others.

Since anharmonic effects may also be present, those relative cross sections that can provide information on the departure from a pure harmonic scheme are of special interest. This is the case for the two cross sections for which both are allowed in the harmonic case but only one of them is forbidden in the rotational or superconductive limit. It is shown that the shell-model approach is a simpler framework for the discussion of these anharmonic effects than the treatment in terms of collective degrees of freedom [4, 5]). This latter approach is probably more fundamental when considered as a contribution to the study of collective states in the nuclear many-body system.

2. Shell-model calculation and energy spectrum

The Hamiltonian that is considered here is

$$\mathscr{H} = \sum_j \varepsilon_j N(j) - G \sum_{j\mu} A_\mu^+(j) A_\mu(j), \tag{1}$$

where ε_j are the single-particle energies and

$$N(j) = \sum_m (n_{jm}^+ n_{jm} + p_{jm}^+ p_{jm}), \qquad A_1^+(j) = \sum_m \frac{(-)^{j-m}}{2} n_{jm}^+ n_{j-m}^+, \tag{2}$$

$$A_0^+(j) = \sum_m \frac{(-)^{j-m}}{2\sqrt{2}} (n_{jm}^+ p_{j-m}^+ + p_{jm}^+ n_{j-m}^+), \qquad A_{-1}^+(j) = \sum_m \frac{(-)^{j-m}}{2} p_{jm}^+ p_{j-m}^+.$$

In eq. (2) $n_{jm}^+(p_{jm}^+)$ are the ordinary fermion creation operators of a neutron (proton) in a state with angular momentum j and z-projection m.

The shell-model states can be classified by specifying the number of pairs in each j-shell and the total isospin to which these are coupled [28]). In the present calculation, only three shells are considered, namely the $1f_{\frac{7}{2}}$, $2p_{\frac{3}{2}}$ and $1f_{\frac{5}{2}}$. The shell-model basis may therefore be written as $|M_1\ M_2(T_1T_2)T_{12}, M_3T_3, TT_z\rangle$ in which T_1 and T_2 are coupled to the intermediate isospin T_{12}. This is an obvious extension of the basis used in ref. [9]) and the matrix elements can easily be calculated along the same lines.

The size of the matrices for the cases of interest, $0 \leqq T \leqq 4$ and $54 \leqq A \leqq 58$ (i.e. $7 \leqq M_1 + M_2 + M_3 \leqq 9$) ranges from † 69 to 151.

† The extension to the four-level case, including the $2p_{\frac{1}{2}}$, increases the size of the matrices to ≈ 700.

The free parameters of the calculation are the two single-particle energies, $\varepsilon_1 = \varepsilon_{1f_{\frac{7}{2}}} - \varepsilon_{2p_{\frac{3}{2}}}$ and $\varepsilon_2 = \varepsilon_{1f_{\frac{5}{2}}} - \varepsilon_{2p_{\frac{3}{2}}}$, and the strength of the pairing force G.

The comparison of the resultant eigenvalues with the empirical energies is made by subtracting the Weizsäcker estimate from the experimental binding energies, choosing the ^{56}Ni ground state to have zero energy:

$$W_{\text{exp}}(T, A) = -B_e(T, A) + B_e(0, 56) + (B_{\text{Coul}}(Z, A) - B_{\text{Coul}}(28, 56)) + (B_{\text{surf}}(A) - B_{\text{surf}}(56)) + (B_{\text{vol}}(A) - B_{\text{vol}}(56)) + B_{\text{sym}}(T, A), \quad (3)$$

$$B_{\text{vol}}(A) = -15.6A, \qquad B_{\text{Coul}} = -0.7Z^2 A^{-\frac{1}{3}}(1 - 0.76Z^{-\frac{2}{3}}),$$

$$B_{\text{surf}}(A) = -17A^{\frac{2}{3}}, \qquad B_{\text{sym}} = 2b_{\text{sym}} A^{-1} T(T+1). \quad (4)$$

There is, however, some ambiguity concerning the symmetry term. Contributions to the T-dependence of the eigenvalues, arising from the shell structure and from the pairing force, are supposed to be contained in the eigenvalues of (1). On the other hand, the T-dependence of the single-particle potential is not included. This is written as

$$V = V_0 + (V_1/A)\, \boldsymbol{t} \cdot \boldsymbol{T}, \quad (5)$$

where $\boldsymbol{t}$ is the nucleon isospin and $\boldsymbol{T}$ is that of the rest of the nucleons. The available analysis [11]) is consistent with values of V_1 ranging from 70 to 110 MeV. This isovector dependence gives rise to a potential part of B_{sym}

$$B_{\text{sym}}(\text{pot}) = \tfrac{1}{2} \sum_i \frac{V_1}{A} \boldsymbol{t}_i \cdot \boldsymbol{T} = \frac{1}{2} \frac{V_1}{A} T^2 \approx 50 A^{-1} T(T+1). \quad (6)$$

This effect should be removed together with the other terms of the Weizsäcker formula. The symmetry term in (3) and (4) is thus reduced to one-half of its usual value [ref. [11])].

Any particular choice of the zero energy for the single-particle levels introduces a corresponding linear dependence on the number of pairs M in the resultant eigenvalues. However, linear effects of the number of particles have been almost completely removed from the empirical energies by including the volume term in the subtraction made † in (3). Therefore, we have also to eliminate the linear term from the theoretical energies. This is accomplished by introducing a term λM in the single-particle Hamiltonian. The Lagrange multiplier λ is obtained together with the only three physically meaningful parameters ε_1, ε_2 and G, by minimizing the expression ††

$$\chi^2 = \sum_k \{(E_k + \lambda M) - (E_0 + \lambda M_0) - W_{\text{exp}}(T_k, A_k)\}^2. \quad (7)$$

† Empirically an optimum symmetry between the levels corresponding to the $A = 54$ and 58 systems is obtained by using in (3) the value $B_{\text{vol}} = 15.48\ A$ MeV.

†† An alternative minimization was performed leaving also b_{sym} as a free parameter. The result obtained [$B_{\text{sym}} = 50.79\ A^{-1}T(T+1)$ MeV] is quite consistent with the conclusions derived from (5) and (6).

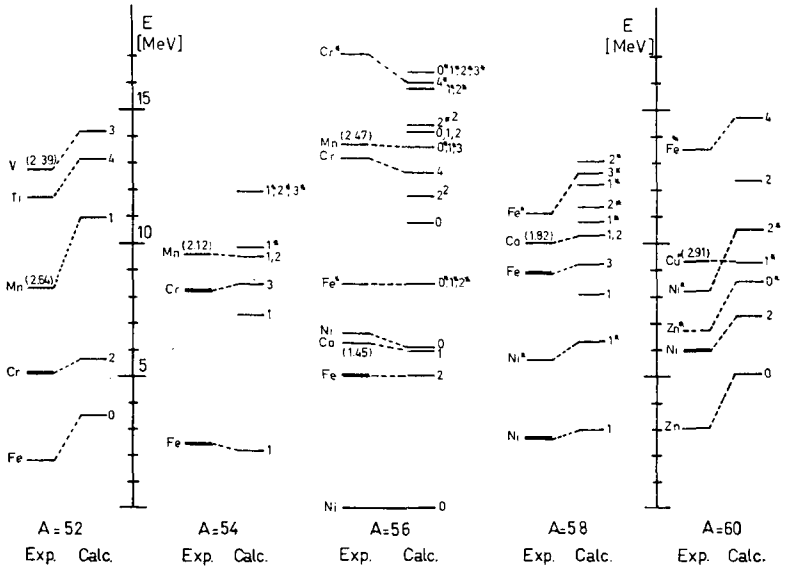

Fig. 1. Theoretical and experimental energy spectra. The numbers at the right of each calculated level stand for the isospin. Non-adiabatic states are indicated by a star. The thick experimental levels correspond to stable isotopes. References to all experimental energies are given in tables 2 and 3, except for ^{58}Ni(2.94 MeV) [ref. [29])].

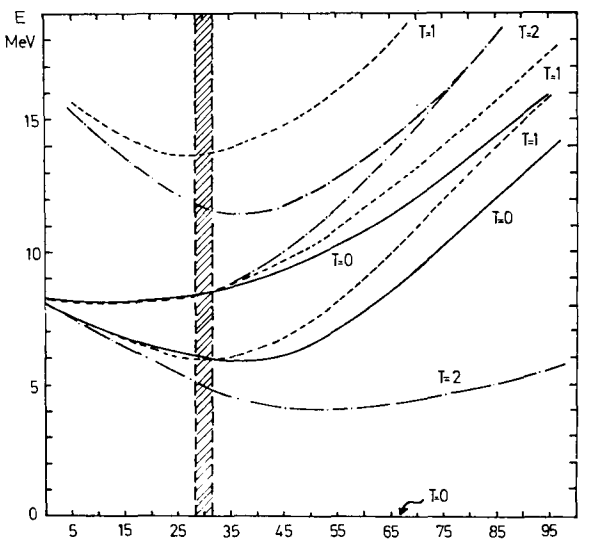

Fig. 2. The lowest $T = 0$ (full line), $T = 1$ (dotted line) and $T = 2$ (dash-dot line) are plotted for $A = 56$ as a function of $G_0 = GA$. The best-fit region (shaded) is seen to correspond to the transitional region.

Here k labels each of the $J^\pi = 0^+$ states under consideration, E_k is the eigenvalue, M_k the number of pairs, T_k the isospin and W_{exp} the empirical energy (3) corresponding to the same state. The subindex $k = 0$ denotes the lowest $T = 0$ eigenvalue for the number of pairs corresponding to ^{56}Ni.

In the summation of (7) we have included only the known levels of the systems $A = 54$, 56 and 58 which may be interpreted within the adiabatic collective description [1]). In fig. 1 these levels are shown, together with ^{56}Fe (3.44 MeV), ^{56}Fe (3.90 MeV), ^{58}Ni (2.90 MeV) and ^{58}Fe(2.26 MeV), which have been excluded from the minimization, since they fall outside the adiabatic description. The best-fit values of the single-particle energies are consistent with the systematics [11]) of the region

$$\varepsilon_1 = -3.97 \pm 0.03 \text{ MeV}, \qquad \varepsilon_2 = 0.25 \pm 0.05 \text{ MeV}. \tag{8}$$

No significant changes are found in the value of χ^2 for variations in ε_1 and ε_2 within the uncertainties given in (8). The best-fit value † of G is given by

$$G = (30 \pm 3) A^{-1} \text{ MeV}. \tag{9}$$

Theoretical and experimental energies are displayed in fig. 1; each state is labelled by the $T_z = T$ member of the isobaric multiplet. The minimum value of χ^2 corresponds to an average departure of 300 keV (4.2 %) per level.

In fig. 2 the lowest $T = 0$, 1 and 2 states for $A = 56$ have been plotted as a function of G. As can be seen from this figure, the value of $G = 30A^{-1}$ MeV corresponds to the transitional region, since the energies of the excited $T = 0$ states have a minimum in this neighbourhood.

In fig. 2, the states appearing right above the two-phonon triplet are interpreted to be associated with the non-adiabatic roots of the RPA. These states do not exist in a two-level model and show a rather small two-particle cross section. They can be individualized in several of the available reaction data.

A simple model may be used to incorporate these states into the collective harmonic description, including a non-adiabatic addition phonon plus the usual removal and addition adiabatic modes. The forward amplitude of the new phonon is an appropriate linear combination of the $(2p_{\frac{1}{2}})^2$ and $(1f_{\frac{1}{2}})^2$ configurations which is out of phase with respect to the two-body transfer process ††.

The wave functions can be written

$$|n_r t_r, (n_a t_a, n'_a t'_a) T_a, T\rangle, \tag{10}$$

which is an obvious extension [1, 3]) of the harmonic notation †††. The primed quantities refer to the non-adiabatic part.

† The same value of $A = 56$ has been used in order to determine the value of G for the three systems $A = 54$, 56 and 58.

†† Since we have only a single j-shell below the Fermi energy for ^{56}Ni there is no possibility of introducing a non-adiabatic removal phonon.

††† The symbols n_i, t_i denote the number of i-phonons and the isospin to which these are coupled, respectively.

In fig. 1 there are several multiplets of states which may be interpreted in terms of configurations involving non-adiabatic phonons, namely,

$n_r = 2, \quad t_r = 0, 2, \quad n_a = t_a = 0, \quad n'_a = t'_a = T_a = 1, \quad T = 1^2, 2, 3$

$(A = 54, \ E = 11 \text{ MeV});$

$n_r = t_r = 1, \quad n_a = t_a = 0, \quad n'_a = t'_a = T_a = 1, \quad T = 0, 1, 2$

$(A = 56, \ E = 8.4 \text{ MeV});$

$n_r = 2, \quad t_r = 0, 2, \quad n_a = t_a = n'_a = t'_a = 1, \quad T_a = 0, 1, 2, \quad T = 0^2, 1^3, 2^3, 3^2, 4$

$(A = 56, \ E > 14 \text{ MeV});$

$n_r = t_r = 1, \quad n_a = t_a = n'_a = t'_a = 1, \quad T_a = 0, 1, 2, \quad T = 0, 1^3, 2^2, 3$

$(A = 58, \ E > 11 \text{ MeV});$

$n_r = t_r = 0, \quad n_a = t_a = n'_a = t'_a = 1, \quad T_a = T = 0, 1, 2 \quad (A = 60, \ E > 10 \text{ MeV}).$

In general our shell-model predictions concerning the energy of the non-adiabatic states (fig. 1) are remarkable accurate, when compared to the experimental data. Including these states the new value of χ^2 corresponds to an average departure of 550 keV per level. This represents a small change, considering that the non-adiabatic states were not included in the determination of the parameters (8) and (9).

The usefulness of the wave function (10) depends on the extent to which the harmonic description is applicable. Since most microscopic calculations yield anharmonic terms that are proportional to some power of the matrix element of the specific operator (in this case the two-body transfer operator), we expect the harmonic description to hold better for the states involving the non-adiabatic phonon than for the adiabatic ones. Indeed, in fig. 1 the splitting between states having $n'_a \neq 0$ is considerably smaller than the splitting between the corresponding states having the same total number of phonons and $n'_a = 0$ (see, for instance, the triplet of states at 8.4 MeV compared to the one at about 6 MeV).

On the other hand, the structure of the shell-model wave function can be studied by means of the numbers

$$a^{\alpha, M, T}(n_1 n_2) = \sum_{\substack{M_2 + M_3 = n_2 \\ T_i}} |C^{\alpha, M, T}_{M_1 = n_1, M_2 M_3 T_i}|^2, \tag{11}$$

where the $C^{\alpha, M, T}_{M_i T_i}$ are the components of the αth eigenvector for a given M and T. The values (12) represent the degree of admixture of states with a higher number of phonons, since the numbers $N_r = 8 - n_1$ and $N_a = n_2$ correspond to the number of removal and addition TDA phonons [1, 2]). In fig. 3 the structure of the three lowest states with $T = 0$ and $A = 56$ has been plotted as a function of G.

For $G = 0$ the dominant configurations have $(n_1, n_2) = (8, 0)$ for the lowest states and $(n_1, n_2) = (7, 1)$ for the next two excited states. As G increases other configura-

tions with a greater number of excited pairs (i.e. with a larger number of addition and removal quanta) mix in the wave function. For $G = 30A^{-1}$ MeV the first excited state has a 4p-4h contribution ($(n_1, n_2) = (6, 2)$) which is larger than the 2p-2h ($(n_1, n_2) = (7, 1)$) contribution. For even larger values of G (corresponding to the "deformed" or superconducting region) there is no predominant configuration.

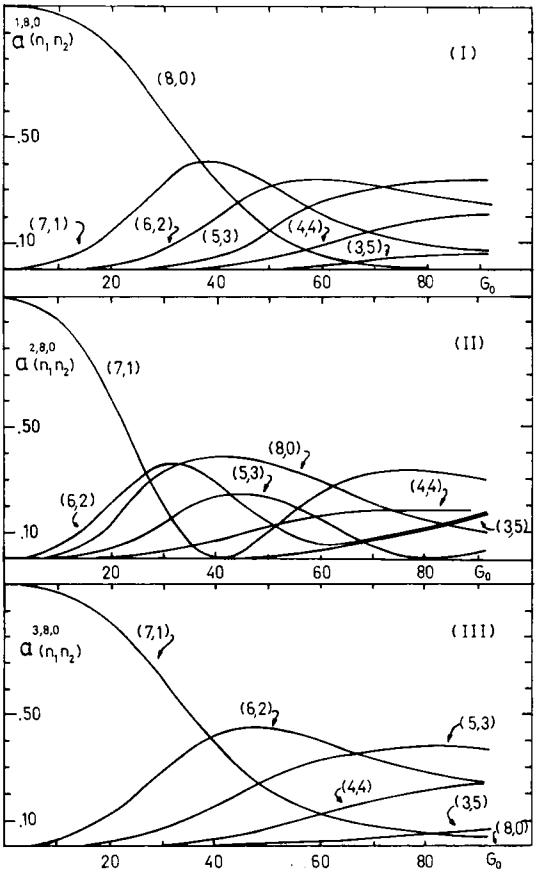

Fig. 3. The structure of the wave function as given by eq. (11) is plotted as a function of G_0, for the three lowest $T = 0$ states for $A = 56$. Plots (I) and (II) correspond to collective states and (III) to a non-adiabatic one. Notice the lower admixture of the wave function (III) as compared to (II).

It is interesting to compare the curves (II) and (III) of fig. 3. Both have a predominant (7, 1) structure for small values of G, the main difference between them being that the configurations implied by $n_2 = 1$ are coherent with respect to the two-body transfer process in case (II) (adiabatic state) and incoherent in case (III) (non-adiabatic state).

As G increases, both states acquire different admixtures. Some of these are due to the RPA mechanism (enhancing transition rates through ground state correlations).

Other admixtures however, are induced by anharmonic terms since, for instance, the predicted (p, t) cross section to this state is considerably smaller than the harmonic prediction (see table 2).

The admixtures are much larger for the adiabatic state (II) than for the non-adiabatic state (III). A similar effect can be systematically found for all states in the vicinity of $A = 56$, therefore confirming the applicability of the harmonic description for the non-adiabatic boson.

3. Analysis of the reaction data

3.1. DWBA CALCULATIONS

The comparison with the two-particle transfer experimental information is performed with the code TWOPAR [12]). The optical parameters are summarized in table 1. The proton parameters are taken from Perey [13]) and ref. [6]), but in (t, p) reactions a further search is made in the depth of the real potential. The results are summarized in fig. 4. From this adjustment we obtain an energy dependence

$$V_R^{(p)} = 56.5 - 0.30E^{(p)}\ \text{MeV}, \tag{13}$$

which is very close to that of ref. [13]), and also consistent with that of ref. [14]). This energy dependence is also used in the analysis of the ^{58}Ni(p, t)^{56}Ni experiment in which the bombarding energy of the protons is 50 MeV.

The triton optical parameters are also taken from ref. [6]). In the triton well no changes with energy are introduced, since the shapes of the angular distributions appear to be quite insensitive to these variations.

The τ optical parameters are taken from ref. [15]). Only an energy dependence in the volume absorptive part is introduced following the pattern of fig. 12 in ref. [15]). The corresponding values are plotted in the upper right-hand corner of our fig. 4.

The neutron parameters are taken from ref. [16]) without any further search.

The two-neutron transfer cross sections given by TWOPAR are multiplied by a factor of 400 in order to reproduce the absolute value in mb/sr of the ^{56}Fe(t, p)^{58}Fe (g.s.) differential cross section. This factor is somewhat larger than the factor 310 of ref. [17]). The difference is probably due to the fact that a relatively smaller set of valence single-particle states is considered here and, therefore, coherent contributions from more distant levels are lost.

The normalization of the proton-neutron transfer is obtained by fitting the differential cross section of the ^{54}Fe(τ, p)^{56}Co$^{T=2}$ reaction. The value obtained (740) is larger than the one corresponding to the two-neutron transfer †.

Regarding the two-proton transfer only relative strengths are available and therefore no analysis is performed of absolute cross sections.

† The normalizations of the proton-neutron transfer processes can be reduced by using the set of τ-parameters given in ref. [19]), which have smaller values of the absorption.

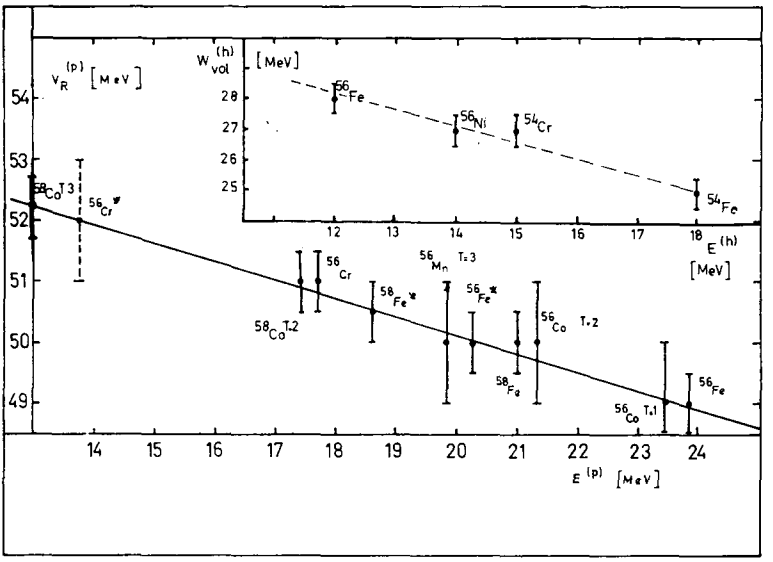

Fig. 4. The real potential depth as a function of the outgoing energy of protons. Any changes within the error bars cause no significant changes in the shape of the angular distributions. The dashed error bar indicates that the experimental angular distribution could not be reproduced. Upper right-hand corner: The absorptive volume potential for the τ-particle as a function of the incident energy. This dependence is suggested in ref. [15]).

TABLE 1

Optical-model parameters

Projectile	R_0 (fm)	A_0 (fm)	V_R (MeV)	R^I_{0V} (fm)	A^I_{0V} (fm)	W^I_V (MeV)	R^I_{0S} (fm)	A^I_{0S} (fm)	W^I_S (MeV)
			[a])						19.5 [d])
p	1.25	0.65	$V_0-0.3E_p$				1.25	0.47	15.5
t	1.16	0.75	165.4	1.5	0.75	16.4			
τ	1.14	0.723	177.0	1.6	0.81	$W(E)$ [a])			
[b])	1.265		42.10				1.238		8.55
n		0.66						0.48	
[c])	1.278		42.53				1.244		8.69

[a]) See text and fig. 5.
[b]) From ref. [16]), used for ^{54}Fe(τ, n)^{56}Ni.
[c]) From ref. [16]), used for ^{58}Ni(τ, n)^{60}Zn.
[d]) Used for (p, t) reactions on ^{58}Ni.

The comparison with experimental data is found in table 2 and figs. 5–8. The quoted empirical results are often a combination of two experiments, for instance an angular distribution given in relative units is cast into an absolute scale using the data measured for a fixed angle in a different experiment.

In all figures where error bars are given, they take into consideration both the statistical error that is reported in each experiment and the uncertainties that are introduced in converting the published material into a standard scale.

In order to obtain the experimental cross sections of table 2, a smooth line is drawn through the empirical points and a summation of the differential cross section is performed between 10° and 90° in steps of 5°. This is done with the purpose of standardizing the experimental data avoiding the uncertainties of extrapolations near zero scattering angle. However, since the largest contributions to the cross section come from the few small angles where the slope of $d\sigma/d\Omega$ is larger, this procedure also induces errors which prevent the extraction of more definite conclusions from the comparisons in table 2. For instance both the angular distributions and the absolute cross sections for the reaction ^{54}Fe(t, p)^{56}Fe(g.s.) are very well reproduced according to fig. 5. However, the small discrepancy between the experimental and theoretical values of the differential cross section at 10° is sufficient to produce the 30 % discrepancy of table 2.

3.2. DISCUSSION

The reaction data are compared not only to the results of the shell-model description but also to those obtained within the framework of the harmonic approximation [refs. [1-3])].

The cross section for the two-particle stripping reaction

$$(\tfrac{1}{2}, t_z)+[n_r t_r, (n_a t_a, n'_a t'_a)T_a, TT_z] \rightarrow (\tfrac{1}{2}, t_{z1})+[n_{r1} t_{r1}, (n_{a1} t_{a1}, n'_{a1} t'_{a1})T_{a1}, T_1 T_{z1}]$$

is related to

$$\sigma_r = \alpha_r \langle T1T_z(T_{z1}-T_z)|T_1 T_{z1}\rangle^2 \langle 1\tfrac{1}{2}(t_{z1}-t_z)t_z|\tfrac{1}{2}t_{z1}\rangle^2 (2T+1) \begin{Bmatrix} T_a & t_r & T \\ 1 & T_1 & t_{r1} \end{Bmatrix}^2 \times \left[\delta_{t_{r1}, t_r+1} \frac{(t_r+1)(n_r+t_r+3)}{2t_r+3} + \delta_{t_{r1}, t_r-1} \frac{t_r(n_r-t_r+2)}{2t_r-1}\right], \quad (14)$$

for the annihilation of a removal quantum, as in ref. [3]).

For the creation of an addition quantum we have

$$\sigma_a = \alpha_a \langle T1T_z(T_{z1}-T_z)|T_1 T_{z1}\rangle^2 \langle 1\tfrac{1}{2}(t_{z1}-t_z)t_z|\tfrac{1}{2}t_{z1}\rangle^2 \times (2T+1)(2T_a+1)(2T_{a1}+1) \begin{Bmatrix} T_a & t_r & T \\ T_1 & 1 & T_{a1} \end{Bmatrix}^2 \begin{Bmatrix} t_a & t'_a & T_a \\ T_{a1} & 1 & t_{a1} \end{Bmatrix}^2 \times \left[\delta_{t_{a1}, t_a+1} \frac{(t_a+1)(n_a+t_a+3)}{2t_a+3} + \delta_{t_{a1}, t_a-1} \frac{t_a(n_a-t_a+2)}{2t_a-1}\right]. \quad (15)$$

The corresponding expression $\sigma_{a'}$ for the creation of a non-adiabatic phonon is obtained from (15) interchanging (n_a, t_a) with (n'_a, t'_a). The values of the constants α_a, α'_a and α_r depend on the microscopic structure of the a-, a'- and r-photons, respectively.

TABLE 2

Reaction data ($54 \leqq A \leqq 58$)

Reaction	E_{inc} (MeV)	E_{exp} (MeV)	T_f	Spectroscopic amplitudes						$\Sigma_{10^\circ}^{90^\circ} d\sigma/d\Omega$ (mb/sr)			Ref.
				$1f_{\frac{7}{2}}$	$2p_{\frac{3}{2}}$	$1f_{\frac{5}{2}}$ [a]	$1f_{\frac{7}{2}}$	$2p_{\frac{3}{2}}$	$1f_{\frac{5}{2}}$ [b]	exp.	th. [a]	th. [b]	
$^{54}Fe(t, p)^{56}Fe$	12	0.0	2	0.470	0.702	0.776	0.402	0.669	0.768	2.40	3.1	2.8	[6, 20]
$^{54}Fe(t, p)^{56}Fe$	12	3.66	2	0.008	−0.677	0.644	0.004	−0.710	0.617	0.82	1.1	1.3	[20]
$^{56}Fe(t, p)^{58}Fe$	12	0.0	3	0.456	0.827	0.955	0.569	0.946	1.086	4.65	4.5	6.0	[6, 21]
$^{56}Fe(t, p)^{58}Fe$	12	2.26	3	0.011	−0.515	0.496	0.004	−0.710	0.617	0.50	0.62	1.2	[21]
$^{54}Cr(t, p)^{56}Cr$	12	0.0	4	0.476	0.829	0.960	0.569	0.946	1.086	9.7	5.4	7.1	[6, 22]
$^{54}Cr(t, p)^{56}Cr$	12	3.9	4	0.010	−0.515	0.492	0.004	0.710	0.617	0.56	0.76	1.5	[22]
$^{58}Ni(p, t)^{56}Ni$	50	0.0	0	0.402	0.669	0.768	0.402	0.669	0.768	0.62 [c]	0.62	0.62	[23]
$^{58}Ni(p, t)^{56}Ni$	50	6.58	0	0.537	−0.016	0.008	0.580	0.152	0.177	0.06 [d]	0.06	0.21	[23]
$^{58}Ni(p, t)^{56}Ni$	50	7.92	1	0.920	0.017	0.032	1.005	0.264	0.307	0.06 [d]	0.12	0.54	[23]
$^{54}Fe(\tau, p)^{56}Co$	18	1.45	1	−0.016	0.573	0.716	0.402	0.669	0.768	0.34	0.54	1.00	[18]
$^{54}Fe(\tau, p)^{56}Co$	18	3.61	2	0.470	0.702	0.776	0.402	0.669	0.768	1.45	1.4	1.25	[18]
$^{56}Fe(\tau, p)^{58}Co$	12	1.82	2	−0.089	0.267	0.536	0.284	0.473	0.543	0.28	0.14	0.42	[19]
$^{56}Fe(\tau, p)^{58}Co$	12	5.75	3	0.456	0.827	0.955	0.569	0.946	1.086	1.8	1.05	1.40	[19]
$^{54}Cr(\tau, p)^{56}Mn$	15	2.47	3	−0.108	0.391	0.557	0.328	0.546	0.627	0.18	0.39	1.09	[24]
$^{54}Cr(\tau, p)^{56}Mn$	15	9.25	4	0.476	0.829	0.960	0.569	0.946	1.086	[e]	1.6	2.10	
$^{54}Fe(\tau, n)^{56}Ni$	14	0.0	0	1.741	0.457	0.531	1.741	0.457	0.531	1 [f]	1	1	[16]
$^{54}Fe(\tau, n)^{56}Ni$	14	6.58	0	−0.016	0.679	0.670	0.402	0.669	0.768	0.7 [f]	1	1.4	[16]
$^{54}Fe(\tau, n)^{56}Ni$	14	7.92	1	−0.016	0.573	0.715	0.402	0.669	0.768	1.8 [f]	1.3	2.3	[16]
$^{54}Fe(\tau, n)^{56}Ni$	14	10.10	2	0.470	0.702	0.776	0.402	0.669	0.768	1.4	0.9	0.8	[16]

[a]) Three-level diagonalization.
[b]) Harmonic approximation.
[c]) No absolute cross sections are available. The experimental ground state intensity is normalized to give the theoretical strength.
[d]) Only an order of magnitude of the relative intensity with respect to the ground state is provided.
[e]) The energy has been obtained from the IAS (^{56}Cr(g.s.)).
[f]) Comparison is based on relative values of $d\sigma/d\Omega$ at 0°.

In order to obtain the spectroscopic amplitudes we have assumed that they should be the same as those of the shell-model calculation for the transitions connecting the ^{56}Ni(g.s., zero phonon) with the ^{58}Ni(g.s., adiabatic addition phonon), with the ^{58}Ni(2.9 MeV, non-adiabatic phonon) and with the ^{54}Fe(g.s., removal phonon). Within the harmonic approximation, the ratio between the three spectroscopic amplitudes is constant for any transition, and thus any other spectroscopic amplitude is obtained from the previous ones by using eq. (14) or eq. (15).

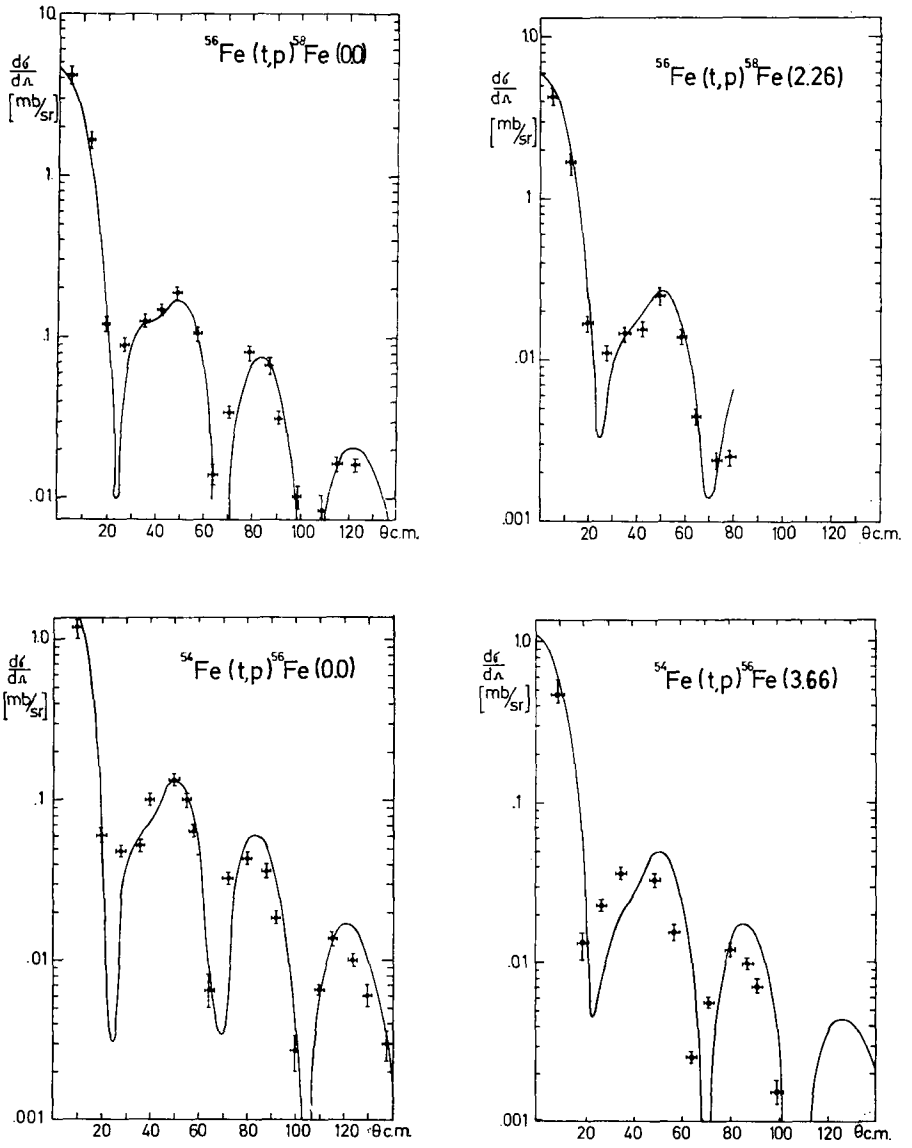

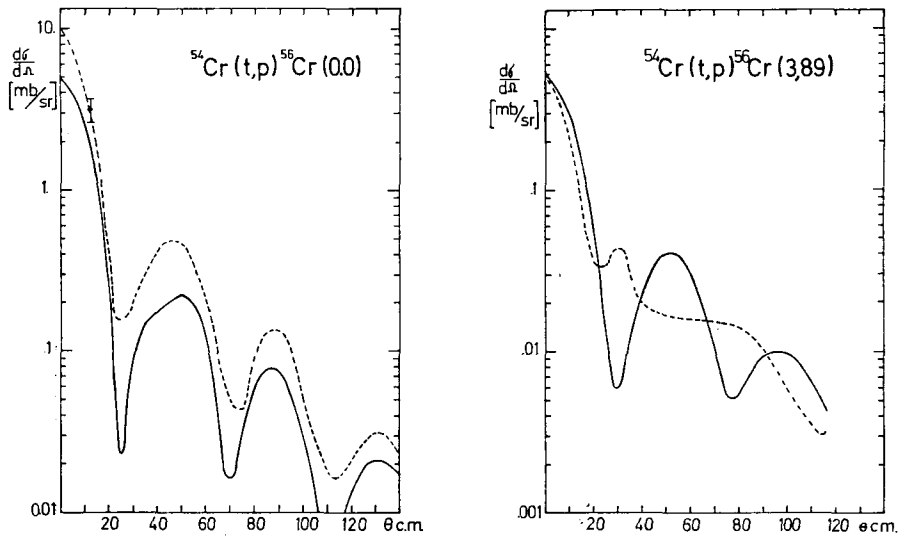

Fig. 5. Angular distributions for (t, p) reactions (A = 54, 56, 58). In this and following figures the full lines are the theoretical angular distributions that are obtained with the spectroscopic factors corresponding to the three-level shell-model diagonalization.

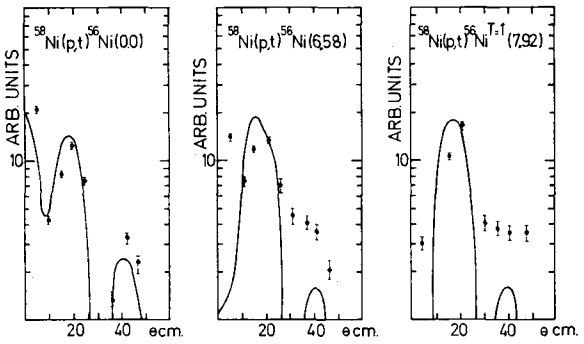

Fig. 6. Angular distributions corresponding to ^{58}Ni(p, t)^{56}Ni. No relative intensities are available.

The spectroscopic factors of both calculations are given in table 2. The shapes of the angular distributions only depend slightly on these numbers and are primarily determined by the optical-model parameters. On the other hand the strengths strongly depend upon the spectroscopic factors, particularly on the one corresponding to the $2p_{\frac{3}{2}}$ orbit.

3.2.1. The (t, p) reactions (fig. 5). The shell-model diagonalization provides results of similar quality to those obtained with the harmonic approximation for those transitions which are allowed in the adiabatic limit. This is to be expected since all these transitions connect states belonging to the same rotational band in the limit of

stable superfluidity. Thus, they are always enhanced, and consequently they are less sensitive to the occurrence of a phase transition.

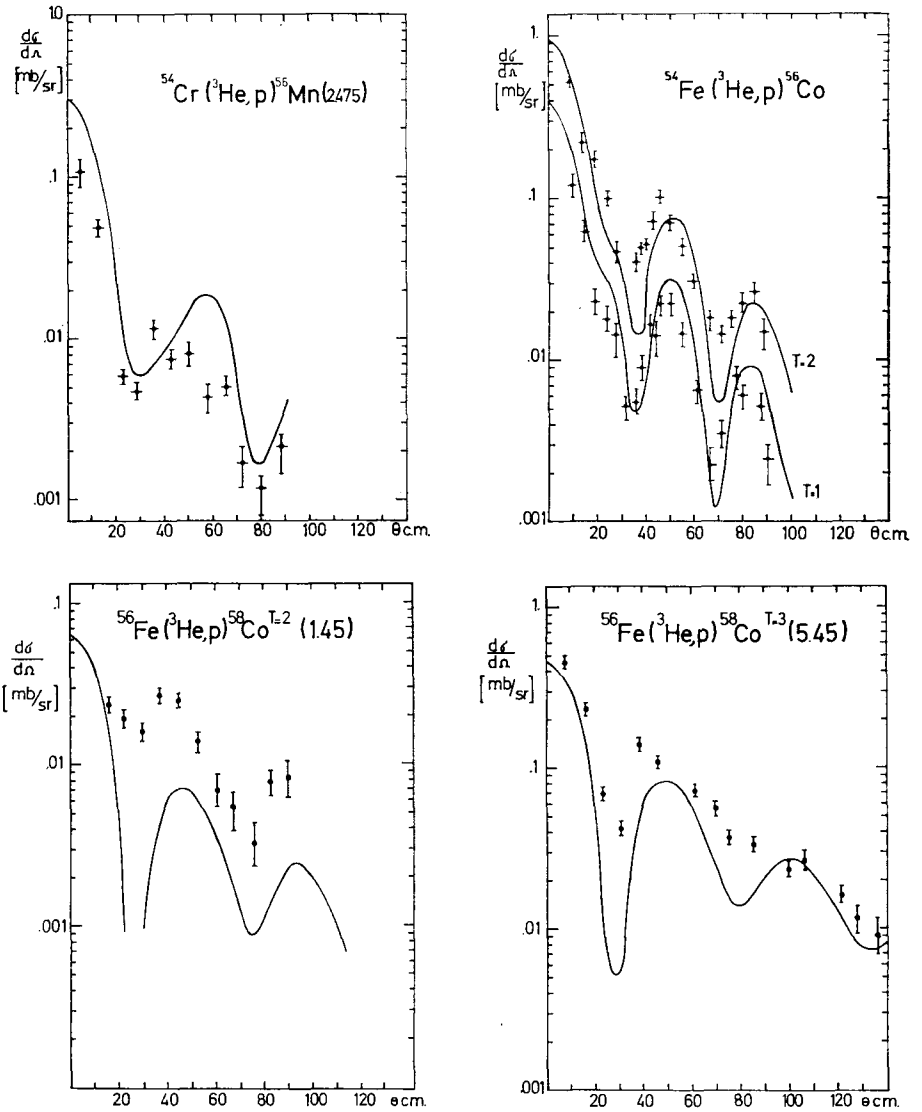

Fig. 7. Angular distributions corresponding to (τ, p) reactions (A = 54, 56, 58).

The non-adiabatic states that were discussed above systematically occur at about 3 MeV of excitation energy. There is an excellent agreement between the experimental cross sections and both theoretical predictions.

3.2.2. The (p, t) reactions (fig. 6). The experimental data concern reactions which are allowed in the harmonic approximation and forbidden in the superconducting

limit. The population of the two lowest members of the excited triplet in ^{56}Ni is predicted by the shell-model calculation within the experimental uncertainties. The harmonic approximation considerably overpredicts the population of the triplet.

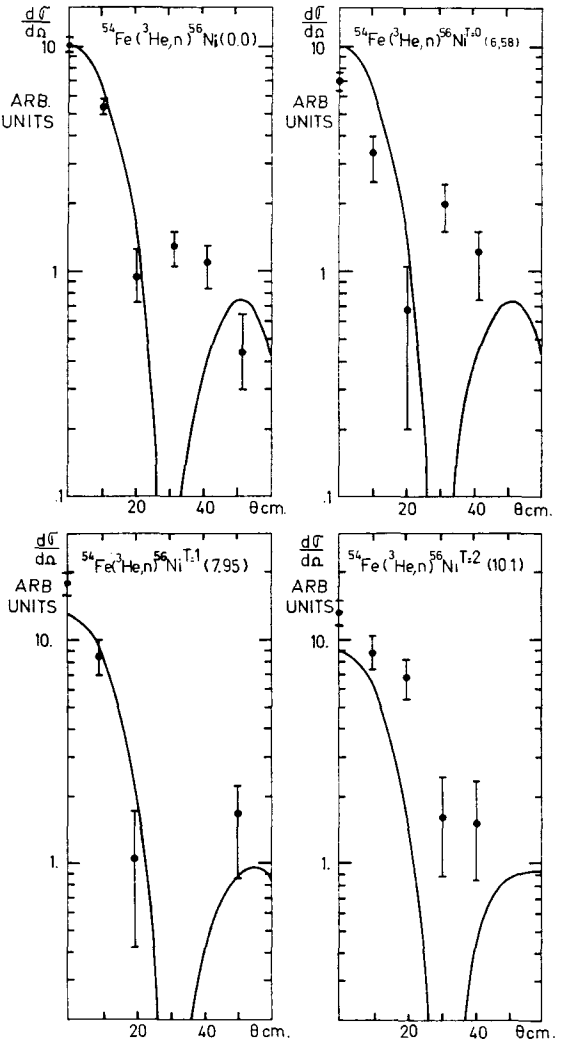

Fig. 8. Angular distributions corresponding to ^{54}Fe(τ, n)^{56}Ni. Only relative intensities are compared.

In the structure of the states given in fig. 3, it can be noted that indeed for $G \approx 30A^{-1}$ MeV the corresponding wave functions are very different from the component (7, 1) that should predominate in the harmonic limit.

A very weak transition populating a state at 4.95 MeV is also reported. This state does not appear in our calculation.

3.2.3. The (τ, p) *reactions* (*fig. 7*). These reactions populate two states having $T = T_t$, $T_t + 1$, respectively where T_t is the isospin of the target. The state with higher isospin is the isobaric analogue (IAS) of the ground state of a neighbouring doubly even nucleus. Experimentally [7]) the population of the state with $T = T_t$ relative to the population of the IAS is systematically smaller by a factor $\frac{1}{3}$ than what is predicted by the harmonic model. This fact may also be interpreted as a phase-transition effect, since these transitions to IAS are allowed in both the harmonic and superconducting limits, while transitions to the $T = T_t$ state should vanish for rigid rotations.

The shell-model calculation accurately predicts † the experimental cross sections listed in table 2.

3.2.4. The (τ, n) *reactions* (*fig. 8*). The (τ, n) reaction populates all the members of the two-phonon vibrational triplet. While the relative strength of the ground with respect to the vibrational state is better reproduced by the three-level description, the intensities within the triplet are slightly better predicted by the harmonic approximation.

4. Extension to $A = 52$ and 60 nuclei

The same calculation of energies and two-particle transfer processes of sect. 3 has been extended to systems involving one pair of particles less and one pair more. The calculation is made with the same values of single-particle energies (8) and pairing strength (1) that yield the previous fit.

The energy eigenvalues are also compared to experiment in fig. 1. The agreement is not as good as for $54 \leqq A \leqq 58$ (the average departure per level increases to 1.19 MeV (15 %)). It must be noted that all the theoretical levels appear to be shifted upwards with respect to experiment by approximately the same amount ††, in all the known cases of $A = 52$ and 60.

The specificity of the wave functions with respect to the pair transfer process may still allow one to come to some conclusions about the structure of the 0^+ levels involved.

The DWBA analysis is performed using the optical-model parameters given in sect. 3. All the results are summarized in table 3 and figs. 9–12.

4.1. REACTIONS ON $A = 58$ NUCLEI LEADING TO $A = 60$

In the ^{58}Fe(t, p)^{60}Fe reaction the only experimental evidence is the absolute cross section of the ground state measured at a c.m. scattering angle of 12.5°. Both the shell

† Recent experimental data [7]) for the reaction ^{54}Fe$(\tau, p)^{56}$Co at 15 MeV incident energy give for the ratio between differential cross sections for this incident energy 0.4 (shell-model calculation) and 0.8 (harmonic approximation).

†† In fact, if a term proportional to the square of the number of pairs outside the $A = 56$ doubly magic nucleus is added in (7), a best χ^2 is found which corresponds to an average departure per level of 0.61 MeV (8 %) ($52 \leqq A \leqq 60$) without impairing the previous fit for $54 \leqq A \leqq 58$. Such a term may arise from a long-range residual force.

TABLE 3

Reaction data ($A = 52, 60$)

Reaction	E_{inc} (MeV)	E_{exp} (MeV)	T_f	Spectroscopic amplitudes						$\Sigma_{10°}^{90°}$ db/dΩ (mb/sr)			Ref.
				$1f_{\frac{7}{2}}$	$2p_{\frac{3}{2}}$	$1f_{\frac{5}{2}}$ [a]	$1f_{\frac{7}{2}}$	$2p_{\frac{3}{2}}$	$1f_{\frac{5}{2}}$ [b]	exp.	th. [a]	th. [b]	
^{58}Fe(t, p)^{60}Fe	13	0.0	4	0.405	0.820	1.029	0.696	1.159	1.330	2.5 [c]	1.5 [c]	2.8 [c]	[6]
^{58}Ni(t, p)^{60}Ni	12.5	0.0	2	0.399	0.832	0.939	0.568	0.946	1.086	3.36 [d]	3.36	4.7	[25]
^{58}Ni(t, p)^{60}Ni	12.5	2.29	2	0.021	−0.507	0.519	0.004	−0.710	0.617	0.10	0.54	1.2	[25]
^{58}Ni(t, p)^{60}Ni	12.5	5.53	2	0.009	0.003	0.072	0.0	0.0	0.0	0.05	0.001	0.0	[25]
^{58}Ni(τ, p)^{60}Cu	13	2.91	1	0.0	−0.704	0.628	0.004	−0.710	0.617	0.17	0.33	0.34	[26]
^{58}Ni(τ, p)^{60}Cu	13	2.54	2	0.399	0.832	0.939	0.568	0.946	1.086	1.7	1.1	1.5	[26]
^{58}Ni(τ, n)^{60}Zn	15	0.0	0	0.734	1.089	1.121	0.568	0.946	1.086	1.0 [e]	1.0 (0.94) [f]	1.0 (0.72) [f]	[16]
^{58}Ni(τ, n)^{60}Zn	15	3.7 [g]	0	−0.055	0.699	−0.767	−0.004	0.710	−0.617		0.16	0.19	[16]
^{58}Ni(τ, n)^{60}Zn	15	7.47	2	0.398	0.832	0.939	0.569	0.946	1.086	0.36	0.33(0.32) [f]	0.61(0.44) [f]	[16]
^{52}Cr(t, p)^{54}Cr	12	0.0	3	0.489	0.713	0.780	0.402	0.669	0.768	3.5	4.0	3.4	[6, 22]
^{52}Cr(t, p)^{54}Cr	12	3.80	3	0.012	−0.680	0.646	0.004	−0.710	0.617	1.3 [h]	1.3	1.5	[22]
^{54}Cr(p, t)^{52}Cr	17.5	0.0	2	0.489	0.713	0.780	0.402	0.669	0.768	8.6	6.4	5.4	[27]
^{54}Cr(p, t)^{52}Cr	17.5	2.48	2	0.871	0.038	0.083	0.899	0.236	0.274	0.53 [i]	0.26 [i]	0.65 [i]	[27]
^{52}Cr(τ, p)^{54}Mn	15	2.12	2	−0.051	0.614	0.696	0.402	0.669	0.768	0.61 [d]	0.61	1.01	[7]
^{52}Cr(τ, p)^{54}Mn	15	6.15	3	0.489	0.713	0.780	0.402	0.669	0.768	1.00	0.97	0.83	[7]

[a]) Three-level diagonalization.

[b]) Harmonic approximation.

[c]) Comparison is based on the value of dσ/dΩ at 12.5°.

[d]) No absolute cross sections are available. The experimental ground state intensity is normalized to give the theoretical shell-model strength.

[e]) Comparison is based on the relative values of dσ/dΩ at 0°.

[f]) The numbers in parentheses are relative intensities at 0° with respect to ^{54}Fe(τ, n)^{56}Ni(g.s.).

[g]) A broad peak has been observed in the cross section at this energy.

[h]) The energy corresponds to the average of three excited states at 2.8, 4.0 and 4.6 MeV. The experimental strength is taken as the sum of the three excited states.

[i]) Comparison is based on the values of $\Sigma_{20°}^{90°}$ dσ/dΩ.

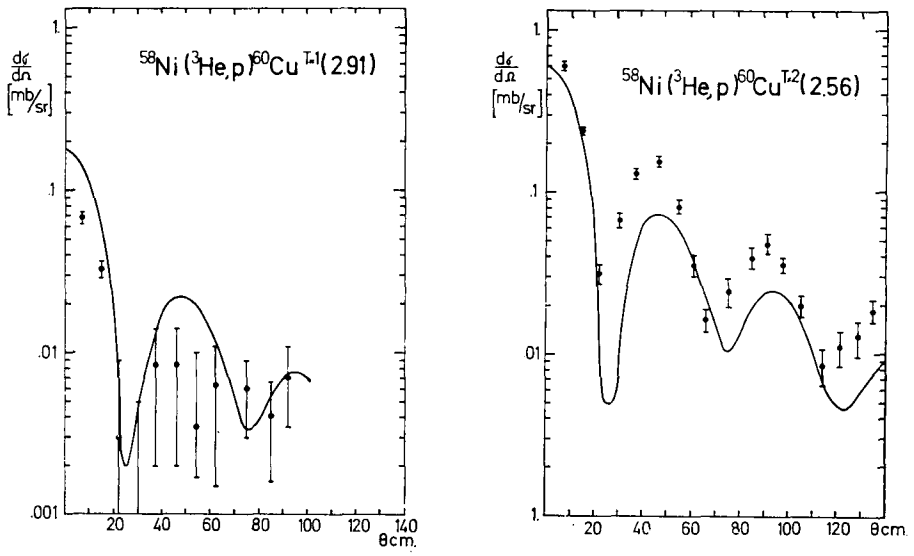

Fig. 9. Angular distributions for ^{58}Ni(τ, p)^{60}Cu.

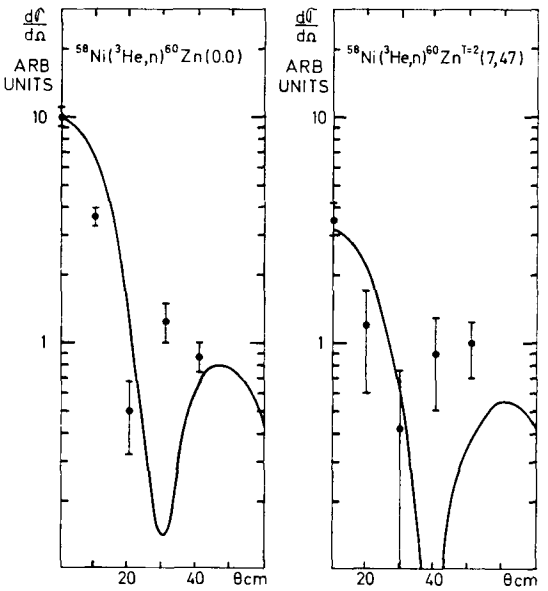

Fig. 10. Angular distributions corresponding to ^{58}Ni(τ, n)^{60}Zn. Only relative intensities are compared.

model and the harmonic calculation hold equally well in the prediction of this cross section. The same considerations of sect. 3 concerning the transitions which are allowed in both the harmonic and rotational limits apply for the above-mentioned

reaction and for the ^{58}Ni(τ, p)^{60}Cu (2.54 MeV, $T = 2$) and for the ^{58}Ni(τ, n)^{60}Zn (7.47 MeV, $T = 2$) reactions (figs. 9 and 10).

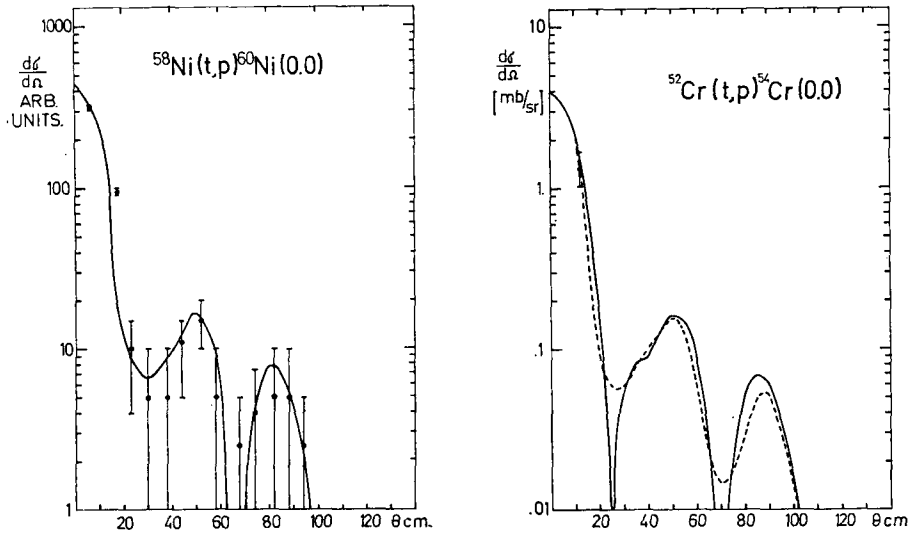

Fig. 11. Angular distributions for (t, p) reactions ($A = 52, 60$). In the ^{60}Ni case the large error bars are due to the conversion from a linear to a logarithmic scale. In this case only the shape of the angular distribution is compared.

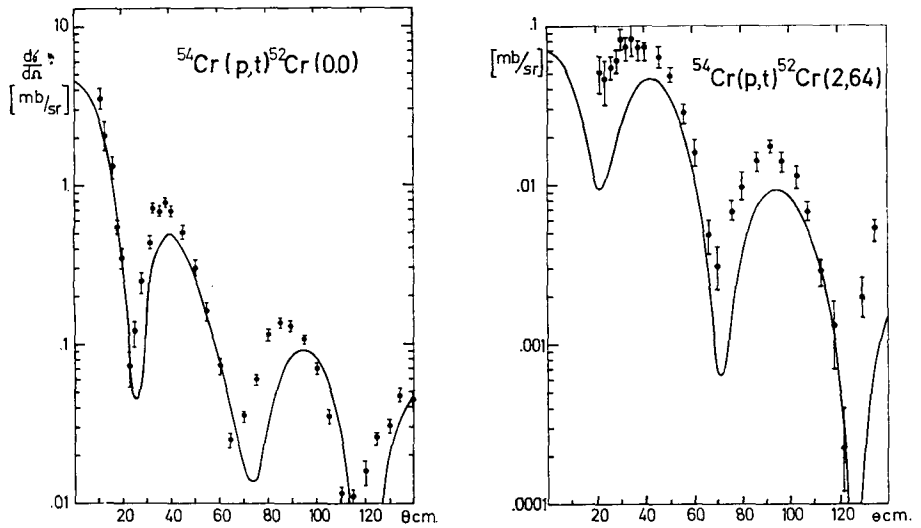

Fig. 12. Angular distributions corresponding to ^{54}Cr(p, t)^{52}Cr.

The lowest populated excited state in ^{60}Ni is interpreted in terms of an adiabatic and a non-adiabatic phonon coupled to $T = 2$. The second excited state shows a

small population and thus probably corresponds to two non-adiabatic phonons. Both the theoretical states at 3.29 MeV and 5.09 MeV excitation energies have a predominant (8, 2) character.

There is a third excited state at 6.36 MeV which is populated with an appreciable intensity. Since the two-phonon energy in ^{56}Ni is $\approx$ 6.5 MeV, the 6.36 MeV state in ^{60}Ni may have this collective character (in this case three addition and one removal phonons). Within this interpretation the 4 % population of this state is a violation of the harmonic oscillator selection rules. The shell-model calculation of the cross section to any state having a (7, 3) character is very small, and therefore does not support this interpretation. It is more likely that at these energies another non-adiabatic phonon involving the $2p_{\frac{1}{2}}$ shell may be responsible for this cross section. The same interpretation probably holds for the ^{58}Ni(τ, n)^{60}Zn (6.88 MeV, $T = 0$) reaction (fig. 10).

The reaction ^{58}Ni(τ, p)^{60}Cu populates a tentative $T = 1$, 0^+ state at 2.91 MeV (fig. 9). This reaction may also be interpreted in terms of a violation of the selection rules concerning the population of levels differing in three phonons. However, again an interpretation in terms of the coupling † between an adiabatic phonon and a non-adiabatic one is more likely, as for the 2.29 MeV state in ^{60}Ni. This interpretation is supported by the shell-model calculation (table 3).

4.2. REACTIONS ON $A = 52$ NUCLEI LEADING TO $A = 54$ AND VICE VERSA

In the ^{52}Cr(t, p)^{54}Cr experiment three excited 0^+ states have been measured at 2.8, 4.0 and 4.6 MeV respectively. These have strengths that are 13 %, 5.6 % and 19 % of the g.s. respectively (table 3). In the shell-model calculation a single excited state is obtained at an energy that approximately coincides with the center of gravity of those states. In order to perform the comparison it is assumed that the corresponding two-particle transfer intensity is fractionated into the three states. The intensity that is obtained theoretically reproduces the sum of the three experimental cross sections. The next theoretical level is at about 6.7 MeV and has a clear three-removal–plus–two-addition phonon structure [about 55 % of the wave function is concentrated in all the configurations having $(n_1, n_2) = (5, 2)$].

No absolute cross sections are available for the reaction ^{52}Cr(τ, p)^{54}Mn$^{T=2,3}$. The shell-model calculation provides a better ratio of the two strengths (table 3) [see the corresponding discussion of (τ, p) reactions in sect. 3].

The ^{54}Cr(p, t)^{52}Cr experimental ground state (fig. 12) intensity is well reproduced by both the shell model and the harmonic calculations. There again are transitions which are allowed in both the vibrational and rotational limits. Within the harmonic scheme two excited states are expected, having $[n_r r_r, (n_a t_a, n'_a t'_a) T_a, T] = [33, (11, 00)\, 1, 2]$ and $[31, (11, 00) 1, 2]$, the latter being much more intensely populated than the first. The eigenvectors of the shell-model diagonalization display also the same struc-

† Note that such a two-phonon state may have the total isospin $T = 1$, since the two addition phonons are not identical.

ture. Although the experimental excitation energy is not consistent with the theoretical predictions for two-phonon excitations, the observed state is associated with the [31, (11, 00)1, 2] configuration, i.e., the more likely to be populated. The relative strength with respect to the ground state is better reproduced by the shell-model calculation. A discussion similar to that of sect. 3 comparing the population of the ground and excited states in ^{56}Ni [via (p, t) and (τ, n) reactions] can also be performed here.

5. Prediction of unreported two-particle transfers

In this section we include spectroscopic amplitudes for the (so far) unreported transitions in the region $52 \leqq A \leqq 60$. As in the previous discussion, these transitions may be divided in to several groups, according to their theoretical relevance:

(a) Transitions AF, which are allowed in the harmonic limit and forbidden in the rotational case.

(b) Transitions FF, which are forbidden in both limits.

(c) Transitions AA, which are allowed in both limits.

(d) Transitions NA, involving non-adiabatic phonons.

For normalization purposes, it is useful to compare the cross sections for AF or FF transitions with the cross sections of AA transitions of the same type leading to the same final nucleus. In cases in which such an AA transition is missing from table 4, it can be found in tables 2 or 3.

Experimental energies are listed in the fourth column, whenever available. These include those obtained from Coulomb energy differences. The energies labelled with the index T are theoretical predictions.

The harmonic classification of the initial and final states (according to eq. (10)) is given in table 4.

6. Conclusion

From the calculations of sects. 2 to 4 it is possible to conclude that the pairing scheme can provide a very good description of the $J^\pi = 0^+$ levels in the nuclei close to $A = 56$.

The fact that the experimental results are better reproduced with values of the pairing strength in the transitional region indicates that the harmonic description may become inapplicable.

Effects associated with the phase transition are not easily detectable in those transitions that are equally allowed in the harmonic and superconducting limits. Indeed, the absolute cross sections for the ground state (t, p) transitions on $^{54, 56, 58}$Fe and on $^{52, 54}$Cr and for the ^{54}Cr(p, t)^{52}Cr(g.s.), ^{56}Fe(τ, p)^{58}Co(5.75 MeV), ^{58}Ni(τ, p) ^{60}Cu(2.91 MeV) reactions and the relative cross sections for the reactions ^{58}Ni(τ, n) ^{60}Zn(g.s. and 7.47 MeV) are equally well reproduced by the shell-model or by the harmonic calculations.

TABLE 4

Spectroscopic amplitudes for the predicted particle transfers

Target	(a, b)B	Final state	E (MeV)	Type	Spectroscopic amplitudes					
					Shell model			Harmonic		
					$1f_{\frac{7}{2}}$	$2p_{\frac{3}{2}}$	$1f_{\frac{5}{2}}$	$1f_{\frac{7}{2}}$	$2p_{\frac{3}{2}}$	$1f_{\frac{5}{2}}$
		11, (00, 00) 0, 1	0.00	AA	1.552	0.331	0.388	1.835	0.482	0.560
^{52}Cr	$(\tau, n)^{54}$Fe	20, (11, 00) 1, 1	5.14^{T}	FF	0.008	0.112	0.128	0.0	0.0	0.0
22, (00, 00) 0, 2		22, (11, 00) 1, 1	7.43^{T}	AF	−0.129	0.662	0.672	0.402	0.669	0.768
	$(\tau, p)^{54}$Mn	22, (00, 11) 1, 2	4.50^{T}	NA	0.001	−0.717	0.640	0.004	−0.710	0.617
		20, (00, 00) 0, 0	0.00	AA	0.901	0.298	0.344	0.820	0.216	0.251
	$(p, t)^{52}$Fe	31, (11, 00) 1, 0	7.37^{T}	FF	0.115	−0.014	−0.008	0.0	0.0	0.0
^{54}Fe		31, (11, 00) 1, 1	2.64	FF	−0.188	0.020	0.021	0.0	0.0	0.0
11, (00, 00) 0, 1	$(p, \tau)^{52}$Mn	22, (00, 00) 0, 2	2.95	AA	1.552	0.331	0.388	1.835	0.482	0.560
	$(\tau, n)^{56}$Ni	11, (00, 11) 1, 0	8.41^{T}	NA	0.008	−0.677	0.644	0.004	−0.710	0.617
	$(\tau, p)^{56}$Co	11, (00, 11) 1, 1	3.93^{T}	NA	0.004	−0.742	0.606	0.004	−0.710	0.617
	$(p, t)^{52}$Cr	33, (11, 00) 1, 2	8.58^{T}	AF	0.073	−0.025	0.007	0.098	0.026	0.030
	$(p, \tau)^{52}$V	33, (11, 00) 1, 3	2.39	AF	0.384	−0.040	−0.025	0.580	0.152	0.177
^{54}Cr		33, (11, 00) 1, 4	8.83	AA	1.345	0.270	0.313	1.974	0.518	0.602
22, (11, 00) 1, 3	$(\tau, n)^{56}$Fe	11, (11, 00) 1, 2	0.00	AA	1.430	0.332	0.382	1.682	0.442	0.513
		11, (00, 11) 1, 2	3.60	FF	0.049	−0.015	−0.081	0.0	0.0	0.0
	$(\tau, p)^{56}$Mn	22, (11, 11) 1, 3	3.71^{T}	NA	0.013	−0.665	0.543	0.003	−0.580	0.503
		22, (11, 11) 2, 3	5.34^{T}	NA	−0.004	−0.146	0.151	0.002	−0.410	0.356
		11, (00, 00) 0, 1	0.00	AA	0.471	0.703	0.776	0.402	0.669	0.768
^{56}Fe	$(p, t)^{54}$Fe	20, (11, 00) 1, 1	5.14^{T}	AF	0.780	0.032	0.069	0.821	0.216	0.250
11, (11, 00) 1, 2		22, (11, 00) 1, 1	7.43^{T}	AF	0.204	−0.020	0.014	0.183	0.048	0.056

		22, (11, 00) 1, 2	2.12	AF	0.570	−0.038	−0.023	0.711	0.187	0.217
^{56}Fe	(p, τ)^{54}Mn	22, (11, 00) 1, 3	6.15	AA	1.430	0.332	0.382	1.682	0.442	0.513
11, (11, 00) 1, 2		00, (11, 00) 1, 1	0.00	AA	1.326	0.385	0.439	1.297	0.341	0.396
	(τ, n)^{58}Ni	00, (00, 11) 1, 1	2.94	FF	0.023	−0.060	−0.082	0.0	0.0	0.0
		11, (20, 00) 0, 1	5.13^{T}	AF	0.051	0.721	0.721	0.424	0.706	0.809
		11, (11, 11) 1, 2	2.90^{T}	NA	0.022	−0.700	0.510	0.003	−0.615	0.534
	(τ, p)^{58}Co	11, (11, 11) 2, 2	4.63^{T}	NA	−0.001	−0.137	0.140	0.002	−0.355	0.308
	(p, t)^{56}Ni	11, (00, 11) 1, 0	8.41^{T}	FF	−0.037	−0.082	0.065	0.0	0.0	0.0
^{58}Ni		11, (11, 00) 1, 1	1.45	AF	0.920	0.018	0.032	1.005	0.264	0.307
00, (11, 00) 1, 1	(p, τ)^{56}Co	11, (00, 11) 1, 1	3.93^{T}	FF	0.036	−0.121	0.091	0.0	0.0	0.0
		11, (11, 00) 1, 2	3.59	AA	1.326	0.385	0.439	1.297	0.341	0.396
		11, (11, 00) 1, 2	0.00	AA	0.456	0.827	0.955	0.569	0.946	1.086
	(p, t)^{56}Fe	11, (00, 11) 1, 2	3.66	FF	−0.074	0.257	0.201	0.0	0.0	0.0
		20, (22, 00) 2, 2	6.77^{T}	AF	0.785	−0.074	−0.008	0.821	0.216	0.250
		22, (22, 00) 2, 3	2.47	AF	0.652	−0.047	−0.048	0.821	0.216	0.250
	(p, τ)^{56}Mn	22, (22, 00) 2, 4	9.25	AA	1.374	0.342	0.392	1.612	0.423	0.492
^{58}Fe		00, (22, 00) 2, 2	0.00	AA	1.232	0.395	0.447	1.189	0.312	0.363
11, (22, 00) 2, 3	(τ, n)^{60}Ni	00, (11, 11) 2, 2	2.29	FF	0.010	0.030	0.049	0.0	0.0	0.0
		11, (31, 00) 1, 2	5.53	AF	0.031	0.691	0.695	0.426	0.708	0.813
		11, (33, 00) 3, 3	2.68^{T}	AF	−0.082	0.100	0.461	0.232	0.386	0.443
	(τ, p)^{60}Co	11, (22, 11) 2, 3	3.08^{T}	NA	0.030	−0.617	0.426	0.004	−0.710	0.617
		11, (33, 00) 3, 4	8.29	AA	0.405	0.820	1.029	0.696	1.159	1.330
	(t, p)^{60}Fe	11, (22, 11) 3, 4	3.33^{T}	NA	0.000	−0.360	0.313	0.004	−0.710	0.617
		00, (11, 00) 1, 1	0.00	AA	0.399	0.832	0.939	0.569	0.946	1.086
	(p, t)^{58}Ni	00, (00, 11) 1, 1	2.94	FF	0.000	−0.241	0.219	0.0	0.0	0.0
^{60}Ni		11, (20, 00) 0, 1	5.13^{T}	FF	0.002	0.000	−0.057	0.0	0.0	0.0
00, (22, 00) 2, 2		11, (22, 00) 2, 2	1.82	AF	0.901	0.004	0.017	1.005	0.264	0.307
	(p, τ)^{58}Co	11, (22, 00) 2, 3	5.75	AA	1.232	0.395	0.447	1.189	0.312	0.363

Experimentally, there are two different effects associated with the existence of a superconducting phase transition. Both involve the comparison of cross sections between a reaction which is allowed in the vibrational and the rotational limit, and a reaction which is forbidden for rigid rotations. The first of them involves the comparison between a (τ, p) reaction in an even target leading to an IAS with $T = T_z + 1$ and a reaction in the same target leading to a $J^\pi = 0^+$ with $T = T_z$ in the same final nucleus. The relative intensity of the latter reaction is about [7]) $\frac{1}{3}$ of the value predicted in the harmonic description. This reduction is well reproduced by the shell-model calculation [see ^{54,56}Fe$(\tau, p)^{58,60}$Co and ^{52,54}Cr$(\tau, p)^{54,56}$Mn].

The second effect of the phase transition lies in the comparison between a ground state transition and a transition to a state which in the harmonic description would have two phonons more than the ground state. Let us look firstly at cases in which the transition to the excited state is allowed. These cases are thus similar to the well-known ^{206}Pb(t, p)^{208}Pb(g.s. and 4.9 MeV) and ^{210}Pb(p, t)^{208}Pb reactions. However, in contrast with the Pb situation, the harmonic description overpredicts the population of the higher state by a factor of ≈ 2 over the experimental value, which is well reproduced by the shell-model calculation [see ^{54}Fe$(\tau, n)^{56}$Ni, ^{58}Ni(p, t)^{56}Ni and ^{54}Cr(p, t)^{52}Cr].

Secondly, we consider those cases in which the population of the excited states is not allowed. These transitions would violate the selection rule $\Delta N = \pm 1$, where N is the number of phonons. No experimental evidence of such anharmonicities has been identified. On the other hand, the corresponding cross sections are predicted to be very small.

The harmonic description works very well in connection with the coupling of a non-adiabatic addition phonon which corresponds to an incoherent linear combination of the $(2p_{\frac{1}{2}})^2$ and $(1f_{\frac{1}{2}})^2$ configurations. Thus it is possible to account for the energy and population of states in ^{54}Cr(3.80 MeV), ^{56}Fe(3.44 MeV), ^{58}Fe(2.26 MeV) ^{56}Cu(3.80 MeV), ^{58}Ni(2.29 MeV) and ^{60}Cu(2.91 MeV) and of a doubtful transition to ^{60}Zn(3.7 MeV). These energies and transitions are also well reproduced within the shell-model calculations. By studying the wave functions in the last calculation (as in fig. 3) it is easy to note the adequacy of the harmonic approximation for the non-collective phonon.

We acknowledge stimulating discussions with Drs. R. A. Broglia, G. G. Dussel and O. Hansen.

Note added in proof: We have learnt that Prof. Hsi-Tseng Chen has also performed an exact calculation of the $T = 1$ pairing force in this region using the methods of ref. [30]).

References

1) A. Bohr, Proc. Int. Symp. on nuclear structure, Dubna, 1968 (IAEA, Vienna, 1968) p. 179
2) O. Nathan, Proc. Int. Symp. on nuclear structure, Dubna, 1968 (IAEA, Vienna, 1968) p. 191
3) B. Bayman, D. R. Bes and R. A. Broglia, Phys. Rev. Lett. **23** (1969) 1299
4) G. G. Dussel, R. P. J. Perazzo, D. R. Bes and R. A. Broglia, Nucl. Phys. **A175** (1971) 513

5) G. G. Dussel, R. P. J. Perazzo and D. R. Bes, Nucl. Phys. **A183** (1972) 298
6) R. F. Casten, E. R. Flynn, O. Hansen and T. J. Mulligan, Phys. Rev. **C4** (1971) 130
7) O. Hansen and O. Nathan, Phys. Rev. Lett. **27** (1971) 1810
8) D. R. Bes, R. A. Broglia and O. Hansen, private communication
9) G. G. Dussel, E. E. Maqueda and R. P. J. Perazzo, Nucl. Phys. **A153** (1970) 469
10) B. F. Bayman and N. M. Hintz, Phys. Rev. **172** (1968) 1113
11) A. Bohr and B. Mottelson, Nuclear structure, vol. 1 (Benjamin, NY, 1969)
12) B. Bayman, Two-nucleon transfer DWBA code TWOPAR, unpublished;
B. Bayman and A. Kallio, Phys. Rev. **156** (1967) 1121
13) F. G. Perey, Phys. Rev. **131** (1963) 745
14) A. Bechetti and G. W. Greenlees, Phys. Rev. **182** (1969) 1190
15) E. F. Gibson, B. W. Ridley, J. J. Kraushaar, M. E. Rickey and R. H. Bassel, Phys. Rev. **155** (1967) 1194
16) R. P. J. Winsborrow and B. E. F. Macefield, Nucl. Phys. **A182** (1972) 481
17) E. R. Flynn and O. Hansen, Phys. Lett. **31B** (1970) 135
18) J. M. Laget and J. Gastebois, Nucl. Phys. **A122** (1968) 431
19) L. L. Lynn, R. C. Shaller, D. A. Barbour, T. A. Belote and W. E. Dorenbusch, Nucl. Phys. **A182** (1972) 272
20) B. L. Cohen and R. Middleton, Phys. Rev. **146** (1966) 748
21) B. L. Cohen, C. L. Fink, J. B. Moorheard and R. A. Moyer, Phys. Rev. **157** (1967) 1033
22) R. Chapman, S. Hinds and A. E. Macgregor, Nucl. Phys. **A119** (1968) 305
23) W. G. Davies, J. E. Kitching, M. McLatchie, D. G. Montague, K. Ramavataram and N. S. Chant, Phys. Lett. **27B** (1968) 363
24) T. Caldwell, D. J. Pullen, T. J. Mulligan and O. Hansen, Nucl. Phys. **A175** (1971) 31
25) F. Darcy, R. Chapman and S. Hinds, private communication
26) H. J. Young and J. Rapaport, Phys. Lett. **26B** (1968) 143, and private communication
27) C. A. Whitten, Jr., Phys. Rev. **156** (1967) 1228
28) K. T. Hecht, Phys. Rev. **139** (1965) B794
29) W. G. Davies, J. E. Kitching, W. McLatchie, J. Morton, D. G. Montague, K. Ramavataram, N. S. Chant, T. A. Hodges, F. Uridge and D. A. Morris, private communication
30) Hsi-Tseng Chen and R. W. Richardson, Phys. Lett. **34B** (1971) 271